IOP Publishing Plasma Sources Science and Technology
Plasma Sources Sci. Technol. **28** (2019) 105004 (10pp) https://doi.org/10.1088/1361-6595/ab3125

A xenon collisional-radiative model applicable to electric propulsion devices: I. Calculations of electron-impact cross sections for xenon ions by the Dirac B-spline R-matrix method

Yang Wang[1], Yan-Fei Wang[2], Xi-Ming Zhu[2,4], Oleg Zatsarinny[3,4] and Klaus Bartschat[3,4]

[1] Department of Physics, Harbin Institute of Technology, Harbin, Heilongjiang 150001, People's Republic of China
[2] School of Energy Science and Engineering, Harbin Institute of Technology, Harbin, Heilongjiang 150001, People's Republic of China
[3] Department of Physics and Astronomy, Drake University, Des Moines, Iowa 50311, United States of America

E-mail: simon.ximing.zhu@outlook.com, oleg.zatsarinny@drake.edu and klaus.bartschat@drake.edu

Received 21 January 2019, revised 21 June 2019
Accepted for publication 5 July 2019
Published 7 October 2019

Abstract

A fully relativistic Dirac B-spline R-matrix (DBSR) method is applied to calculate the oscillator strengths and electron-impact excitation cross sections involving the $5s^25p^5$, $5s5p^6$, $5p^46s$, $5p^45d$, $5p^46p$, and $5p^47s$ states of a Xe^+ ion. A fully relativistic approach is necessary for this problem, since the spin–orbit coupling is of the same order as electron correlations in the outer shells of Xe^+. Also, there is a complex open-shell structure with strong term dependence in the one-electron orbitals. The oscillator strengths are also calculated and agree well with available experimental measurements. We select some important excitation cross sections out of the ground, metastable, and quasi-metastable states of Xe^+ for the collisional-radiative (CR) model to be discussed and analyzed. The present paper is the first one of a series of studies on a CR model of xenon ions in plasma diagnosis and numerical simulations of Hall and ion thrusters. In subsequent papers, the cross-section data for the Xe^+ ion, together with those for neutral Xe from our previous calculation, are used to build a comprehensive CR model for electric propulsion systems involving xenon. Furthermore, the predictions of this model will then be examined by experiments in both Hall and ion thrusters.

Supplementary material for this article is available online

Keywords: xenon ion, cross sections, electron impact, collisional-radiative model, Dirac B-spline R-matrix method, close-coupling

1. Introduction

Xenon has been the most widely-used working gas in the area of electric propulsion systems since the 1990s to the present day, because of its advantages associated with a low ionization threshold, chemical inertness, and nontoxicity [1–3]. Also, it is an important trace gas in the optical line-ratio method for low-temperature plasma diagnostics [4–7], plays a role in fusion research [8] and is related to astrophysics when studying stellar atmospheres [9, 10]. To build a plasma model

[4] Authors to whom any correspondence should be addressed.

for the above topics, oscillator strengths and collisional cross sections involving excited states of Xe and Xe^+ are required. There are a number of experimental and theoretical studies on Xe in the literature [11–16]. Theoretical and experimental reports of Xe^+ oscillator strengths can also be found in the literature [17–22]. However, a detailed investigation concerning the electron-impact excitation cross sections of Xe^+ is very limited. The only available data are from the recent calculations by the fully relativistic distorted-wave (RDW) method by Gupta *et al* [23].

The difficulties in the calculation of cross sections for electron collisions with Xe^+ originate from the complicated structure of this target. As a heavy ion, Xe^+ exhibits a strong term dependence of the orbitals in the $5p^4nl$ outer-shell configurations as well as strong spin–orbit interaction effects that result in substantial fine-structure splittings. Inner-core and core-valence correlation and relaxation effects are also important, especially for transitions from the ground state. The above issues pose great challenges on all theoretical methods, but especially on those using orthogonal bases of one-electron orbitals. As mentioned above, a fully relativistic approach, e.g., the Dirac-Fock method, should be employed when dealing with Xe^+. This becomes very complicated due to the complex open-shell structure.

The present work is the first part of a series on developing a collisional-radiative model for Xe electric propulsion devices. Here we perform a comprehensive investigation regarding the electron-impact excitation cross sections of the Xe^+ ion by using the Dirac *B*-spline *R*-matrix (DBSR) method, which was already employed previously in benchmark calculations of oscillator strengths and electron-impact excitation cross sections of the neutral Xe atom [15, 24]. This theoretical approach achieved a breakthrough in the description of both the target structure problem and the near-threshold resonance phenomena seen in the cross sections for such a complex target. We employ the Dirac–Coulomb Hamiltonian to describe both the *N*-electron target and the $(N + 1)$-electron collision systems. The distinguishing features of the DBSR method are (i) the ability to use term-dependent, and hence nonorthogonal, sets of one-electron orbitals or Dirac spinors in the target description and (ii) *B*-splines as the fundamental basis to expand the wave function of the projectile. The nonorthogonal orbitals provide a vastly increased flexibility and, consequently, accuracy in the target description. There is also great flexibility in the choice of the radial grid in a *B*-spline basis, and machine accuracy may be achieved with simple Gaussian quadrature. Finite-difference algorithms are avoided and well-established linear-algebra packages are used instead. On the other hand, setting up and then diagonalizing the Hamiltonian matrix is complicated, and large-scale calculations like the present one require significant computational resources.

This paper is organized as follows. The numerical approach applied to e-Xe^+ collisions is briefly summarized in section 2. References to more details are provided for interested readers. Results for the target structure (energy levels and oscillator strengths) and cross sections are presented and discussed in section 3. Finally, conclusions and an outlook to future work are given in section 4.

2. Summary of the computational method

The calculations performed for this work employ the fully relativistic DBSR method. It is based on the close-coupling expansion for the total (projectile plus target) wave function for the collision system. A write-up of the semi-relativistic version of the method and the associated computer program was published by Zatsarinny [25] and the extension to the fully relativistic framework was described in detail by Zatsarinny and Bartschat [26]. Many examples of its application can be found in the review [27].

In this work, we use 67 discrete states of Xe^+ in the close-coupling expansion, with dominant configurations $5s^25p^5$, $5s5p^6$, $5p^46s$, $5p^45d$, $5p^46p$, and $5p^47s$, respectively. An *R*-matrix radius $a = 50\ a_0$ ($a_0 = 0.529 \times 10^{-10}$ m, Bohr radius) is chosen and the target Hamiltonian is diagonalized in this box. This choice allowed us to obtain a sufficiently good description for the low-lying bound states of Xe^+ ion (see table A1 in appendix A). Partial-wave contributions up to $J = 50$ are numerically calculated, and no extrapolation scheme to account for even higher partial waves is needed in this work. The present calculations included up to 306 coupled scattering channels, and interaction matrices with dimensions of about 50 000 needed to be diagonalized for each partial wave. In order to perform those calculations, we parallelized the DBSR code and also used parallelized linear-algebra libraries such as SCALAPACK[5].

The detailed computational approach for the DBSR method based on the fully relativistic framework can be found in our previous works [26, 27].

3. Results and discussion

This section presents the structure and cross-section data calculated in this work. In section 3.1, theoretical energy levels and oscillator strengths are compared with experimental and recommended results in the literature. Sections 3.2 and 3.3 exhibit selected electron-impact excitation cross sections of the excited ionic states from the ground state as well as the metastable and 'quasi-metastable' states, where the latter are characterized by having relatively long lifetimes (about 1 μs). These states play important roles in the collisional-radiative (CR) model to be developed and discussed in subsequent papers. Potential limitations of our theoretical approach are discussed in section 3.4.

3.1. Energy levels and oscillator strengths

Table A1 in appendix A shows the energy levels of Xe^+ obtained in the present calculation. The excitation energies

[5] A detailed description of SCALAPACK can be found at http://netlib.org/scalapack/.

Table 1. Comparison of selected oscillator strengths for excitation of Xe^+ from $5p^4 6s$ to $5p^4 6p$ in the velocity (V) and length (L) forms. λ denotes the wavelength of the optical transition.

						This work	
Lower level	Upper level	λ (nm)	PAD[a] [17]	HCL[b] [18]	NIST [20]	V	L
$5p^4(^3P_2)6s\ ^2[2]_{3/2}$	$5p^4(^3P_2)6p\ ^2[1]^\circ_{3/2}$	460.3	0.239	—	0.26	0.238	0.323
$5p^4(^3P_2)6s\ ^2[2]_{5/2}$	$5p^4(^3P_2)6p\ ^2[3]^\circ_{7/2}$	484.4	0.408	0.540	0.52	0.517	0.586
$5p^4(^3P_0)6s\ ^2[0]_{1/2}$	$5p^4(^3P_0)6p\ ^2[1]^\circ_{3/2}$	488.4	0.480	—	—	0.569	0.641
$5p^4(^3P_2)6s\ ^2[2]_{5/2}$	$5p^4(^3P_2)6p\ ^2[2]^\circ_{5/2}$	529.2	0.380	0.403	0.37	0.404	0.462
$5p^4(^3P_2)6s\ ^2[2]_{5/2}$	$5p^4(^3P_2)6p\ ^2[2]^\circ_{3/2}$	533.9	0.191	0.187	—	0.193	0.216
$5p^4(^3P_2)6s\ ^2[2]_{3/2}$	$5p^4(^3P_2)6p\ ^2[3]^\circ_{5/2}$	541.9	0.429	0.452	0.41	0.548	0.614
$5p^4(^3P_1)6s\ ^2[1]_{3/2}$	$5p^4(^3P_1)6p\ ^2[0]^\circ_{1/2}$	543.9	0.153	—	0.16	0.191	0.222
$5p^4(^1D_2)6s\ ^2[2]_{3/2}$	$5p^4(^1D_2)6p\ ^2[3]^\circ_{5/2}$	627.1	—	—	0.16	0.130	0.139

[a] PAD means pulsed arc discharge, which was used as the light source in [17] to determine the Einstein coefficients experimentally. Data marked PAD were converted from these Einstein coefficients.
[b] HCL means hollow cathode lamp. It was used to determine the Einstein coefficients experimentally in [18], and marks oscillator strength values from these data.

Table 2. Comparison of selected oscillator strengths for excitation of the Xe^+ ion from $5p^4 5d$ to $5p^4 6p$, as obtained in the velocity (V) and length (L) forms of the electric dipole operator.

						This work	
Lower level	Upper level	λ (nm)	PAD [17]	HCL [18]	NIST [20]	V	L
$5p^4(^3P_2)5d\ ^2[3]_{7/2}$	$5p^4(^3P_1)6p\ ^2[2]^\circ_{3/2}$	488.7	0.096	—	—	0.128	0.157
$5p^4(^3P_2)5d\ ^2[3]_{7/2}$	$5p^4(^3P_1)6p\ ^2[1]^\circ_{3/2}$	498.9	0.156	—	—	0.100	0.125
$5p^4(^3P_2)5d\ ^2[3]_{7/2}$	$5p^4(^3P_0)6p\ ^2[1]^\circ_{3/2}$	530.9	0.094	—	—	0.060	0.068
$5p^4(^3P_2)5d\ ^2[2]_{5/2}$	$5p^4(^3P_2)6p\ ^2[3]^\circ_{7/2}$	546.0	0.038	0.036	—	0.015	0.025
$5p^4(^3P_2)5d\ ^2[3]_{7/2}$	$5p^4(^3P_2)6p\ ^2[3]^\circ_{5/2}$	553.1	—	0.029	0.030	0.014	0.026
$5p^4(^3P_2)5d\ ^2[2]_{5/2}$	$5p^4(^3P_2)6p\ ^2[2]^\circ_{5/2}$	603.6	—	0.046	0.041	0.033	0.070
$5p^4(^3P_2)5d\ ^2[3]_{7/2}$	$5p^4(^3P_2)6p\ ^2[2]^\circ_{5/2}$	605.1	0.085	—	0.070	0.046	0.086
$5p^4(^3P_2)5d\ ^2[2]_{5/2}$	$5p^4(^3P_2)6p\ ^2[2]^\circ_{3/2}$	609.8	—	0.073	0.097	0.038	0.068
$5p^4(^3P_2)5d\ ^2[2]_{3/2}$	$5p^4(^3P_2)6p\ ^2[2]^\circ_{5/2}$	627.8	—	0.042	0.032	0.020	0.038

from the ground state are compared with those given in the NIST tables [20]. While not perfect, the overall agreement is satisfactory, with the deviations not exceeding a few percent. In the subsequent collision calculation, we adjusted the excitation energies to the NIST values. Since we do not force orthogonality between the target and the projectile orbitals, we do not have to include (N + 1)-electron 'bound–bound' terms in the close-coupling expansion of the collision problem. As a result, using the experimental thresholds does not carry the danger of otherwise possible inconsistencies in the relative positions of the N-electron target and the (N + 1)-electron resonance states. Therefore, the effect of this correction is generally small, especially on the rate coefficients to be calculated from the cross sections, but it is beneficial in making a direct comparison with experiment possible. The energy levels of all states included in the calculation are available on request.

The oscillator strengths, and the related Einstein coefficients, are the fundamental radiative data for building a CR model. In the present work, we calculated oscillator strengths for transitions between all states of the Xe^+ ion that were included in the close-coupling expansion for the collision problem. Note that the 6d states are included when dealing with the target states of Xe^+ and the oscillator strengths are also generated at the same time; however, they are not included in the cross section calculation below considering the limit in the available computational resources. Some of the oscillator strength data are obtainable by analyzing the spectral lines from plasma sources and thus can be used to evaluate the accuracy of our calculation, as listed in tables 1–3.

Table 1 compares the oscillator strengths for several important 6s–6p excitations. Specifically, we show our theoretical values obtained in the velocity and length forms of the electric dipole operator, the values determined from the experimental Einstein coefficients reported in references [17] (using a pulsed arc discharge, PAD) and [18] (using a hollow cathode lamp, HCL), and the data recommended by NIST [20]. Table 2 compares similar data for some 5d–6p excitations. For both groups, the theoretical values are in agreement with the experimental and recommended data (we take the mean value of V and L forms for comparison). The oscillator strengths for the 5d–6p transitions are generally smaller than those for the 6s–6p excitations. However, there are several metastable states in the 5d group, and hence the 5d–6p excitation channels can also be important in Xe plasmas. Even though the 6d states were not included in the collision model, we generated structure data for these states as well.

Table 3. Selected oscillator strengths for excitation of the Xe^+ ion from $5p^4 6p$ to $5p^4 6d$, as obtained in the velocity (V) and length (L) forms of the electric dipole operator.

				This work	
Lower level	Upper level	λ(nm)	LPP[a] [19]	V	L
$5p^4(^3P_1)6p\ ^2[0]^\circ_{1/2}$	$5p^4(^3P_1)6d\ ^2[1]_{1/2}$	415.8	0.374	0.397	0.441
$5p^4(^3P_2)6p\ ^2[2]^\circ_{3/2}$	$5p^4(^3P_2)6d\ ^2[2]_{3/2}$	418.0	0.328	0.335	0.374
$5p^4(^3P_1)6p\ ^2[2]^\circ_{3/2}$	$5p^4(^3P_1)6d\ ^2[3]_{5/2}$	422.3	0.498	0.296	0.348
$5p^4(^3P_0)6p\ ^2[1]^\circ_{3/2}$	$5p^4(^3P_0)6d\ ^2[2]_{5/2}$	439.3	0.942	0.631	0.709

[a] LPP means laser-produced plasma. It is used to measure Einstein coefficients in [19], and marks oscillator strength values from these data.

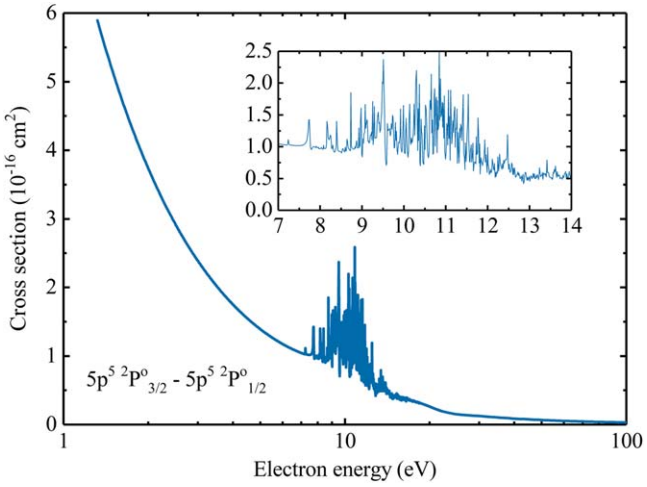

Figure 1. Electron-impact excitation cross section for the $5p^5\ ^2P^o_{3/2}$–$5p^5\ ^2P^o_{1/2}$ transition in Xe^+.

Table 3 lists some oscillator strengths for 6p–6d transitions, which are compared with those measured in a laser-produced plasma (LPP) [19].

Based on the above calculation, a comprehensive set of Einstein coefficients for excited states of Xe^+, which is currently not available in the literature or in the NIST database, will be used for our collisional-radiative model for Hall and ion thrusters. By comparing the modelled and measured branching ratios of Xe^+ emission lines, the accuracy of the calculation can be examined. Preliminary results suggest that the present model is, indeed, sufficient for the purpose of the present study. More details will be reported in follow-up papers.

3.2. Excitation from the ground state

Electron-impact excitation cross sections of $5s^25p^5$, $5s5p^6$, $5p^46s$, $5p^45d$, $5p^46p$, and $5p^47s$ states of Xe^+ were calculated by the DBSR model summarized in section 2. Figure 1 depicts the cross section for the transition between the $5p^5\ ^2P^o_{3/2}$ and $5p^5\ ^2P^o_{1/2}$ states at electron energies below 100 eV. The cross section generally decreases as the electron energy increases. However, temporary atomic states of Xe can be formed in the collision between the projectile electron and the Xe^+ ion, thereby leading to a wealth of resonances in the energy dependence of the cross section. The resonant structure starts at ~8 eV, due to the first excited $5p^5(^2P^o_{3/2})6s\ ^2[3/2]^o_2$ state of atomic Xe. The curve becomes smooth again above 18.57 eV, which is the threshold of the highest-lying state in the present close-coupling expansion.

The cross sections involving the 6s and 5d states in Xe^+ are important for two reasons: (i) the densities of several 5d metastable states and 6s quasi-metastable states can be relatively high in plasmas and hence play important roles for electron-impact excitation and ionization, and (ii) vacuum ultraviolet (VUV) photons emitted by the resonance states in the 6s and 5d groups are involved in photoionization and plasma-surface interaction. Figure 2 shows the excitation cross sections of selected 6s and 5d states from the ground state. The curves involving states with a ^3P core exhibit high peaks near threshold. This may lead to large excitation rate coefficients when the mean electron energy is ~10–20 eV, as found in the ionization region of Hall thrusters [28]. A large amount of metastable (e.g. $(^3P_2)5d\ [4]_{9/2}$ in figure 2(b)) and quasi-metastable (e.g. $(^3P_2)5d\ [2]_{5/2}$ in figure 2(a)) ions can be produced and may contribute to the formation of Xe^{2+} and Xe^{3+} ions, as observed in [29, 30]. The 6s and 5d states with a ^1D core also have relatively large cross sections. In particular, the $(^1D_2)5d\ [2]_{5/2}$ state, exhibited in figure 2(b), shows a flat energy dependence of the cross section with a significant magnitude. This is the typical signature of a resonant transition. On the other hand, the cross sections for states with a ^1S core are relatively small.

A comparison has been made between the present DBSR results and the only (to our knowledge) available theoretical calculations on the e-Xe^+ case by the RDW method of Gupta *et al* [23]. As an example, figure 3 demonstrates the comparison for selected 6s and 5d states. The results of both theoretical methods show some qualitative agreement with each other, especially for the 6s states figure 3(a). There are significant differences in the magnitude between the curves of DBSR and RDW for the $(^1S_0)5d[2]_{5/2}$ and $(^1D_2)5d[2]_{5/2}$ states, as seen in figure 3(b). However, their energy dependences still resemble each other.

Generally, one would expect the RDW method to perform well for the optically allowed transitions at relatively high energies (a few times the ionization threshold and above), when the cross sections are comparatively large. However, for the complex target Xe^+, the channel coupling mechanism plays a significant role, which is neglected in the RDW calculation.

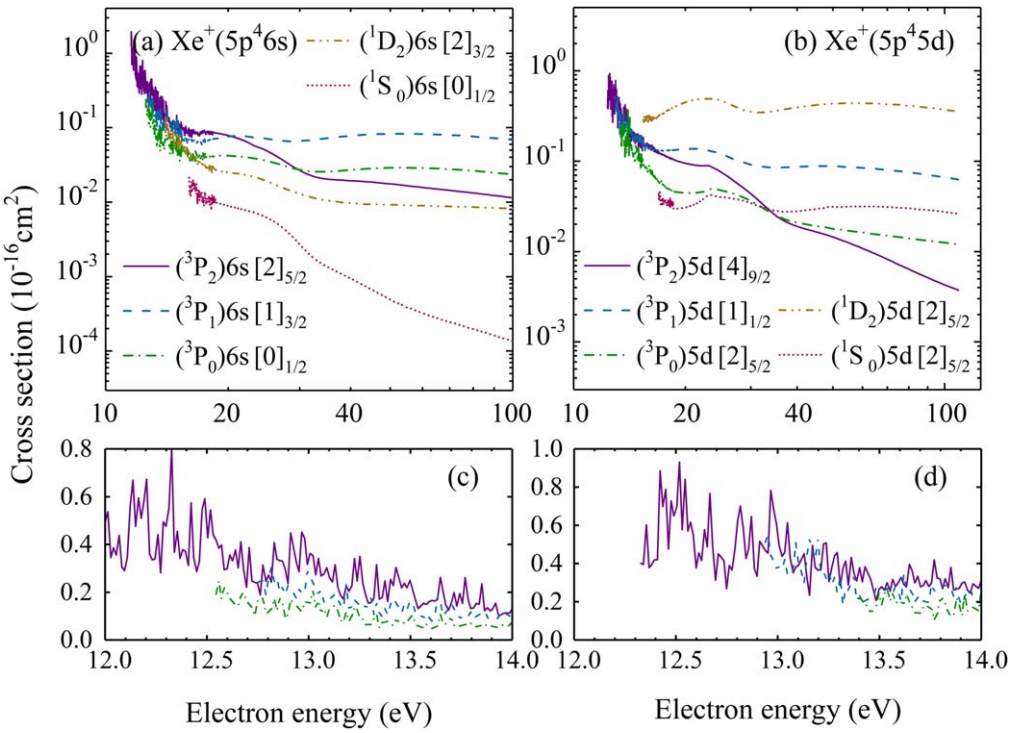

Figure 2. Electron-impact excitation cross sections for transitions from $5p^5\ ^2P^o_{3/2}$ to selected $5p^4$6s (a) and $5p^4$5d (b) states. For brevity the notation has been shortened in the legend, e.g., from $5p^4(^3P_2)6s\ ^2[2]_{5/2}$ to $(^3P_2)6s\ [2]_{5/2}$, etc. Panels (c) and (d) show the near-threshold results on a linear scale.

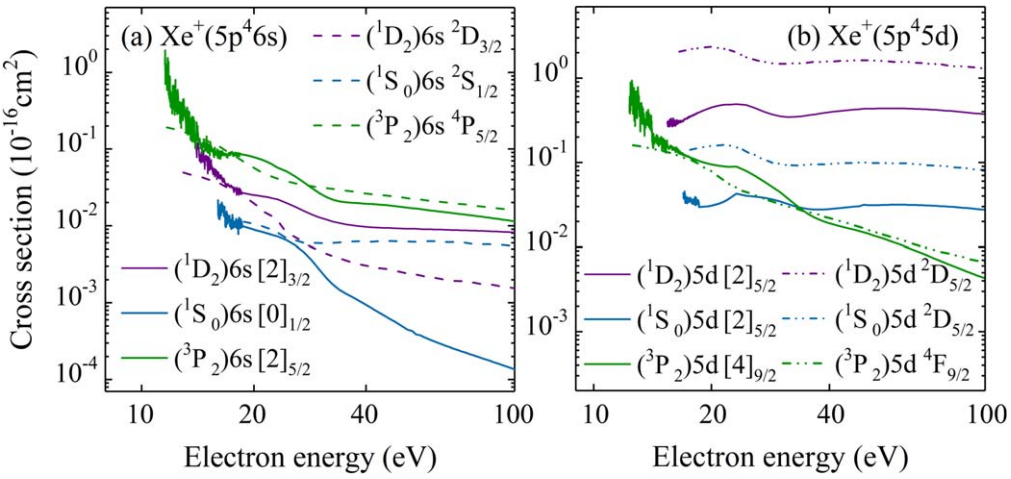

Figure 3. Electron-impact excitation cross sections for transitions from $5p^5\ ^2P^o_{3/2}$ to selected $5p^4$6s (a) and $5p^4$5d (b) states. Solid lines represent the present DBSR calculations; dashed lines denote the RDW calculations by Gupta *et al* [23].

Actually, it is not straightforward to predict how long channel coupling is needed for Xe^+. To investigate this problem and check the stability of the DBSR predictions, we ran the calculations with a smaller number of states and compared the results. While a notable model dependence exists for some transitions (generally when the cross sections are small), we believe that the current DBSR predictions are sufficiently accurate. These data will be used in the collisional-radiative (CR) model and examined by optical experiment in a follow-up paper.

The situation is similar for the other transitions, which are not shown here due to the length limit for the paper. Being based on a non-perturbative approach the DBSR method resolves the detailed resonant behavior of the cross sections in the near-threshold regime, which meets the needs of the CR model for xenon ions in our subsequent research.

As discussed above, the excited configurations $Xe^+(5p^4nl)$ can be divided into three subgroups corresponding to the ^3P, ^1D and ^1S core states of the $5p^4$ configuration. As shown in the examples, the levels with the ^3P core tend to have larger cross sections than those with the other cores. In addition to the propensities associated with angular-momentum coupling (orbital and spin), as well as the parities of the initial and final states, one expects the size of the cross

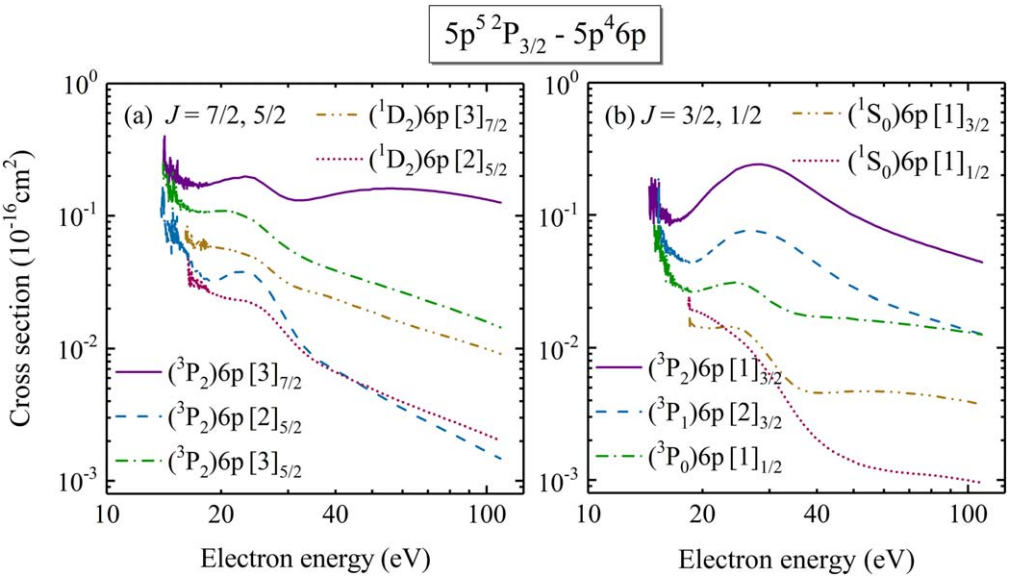

Figure 4. Electron-impact excitation cross sections for transitions from $5p^5\ ^2P^o_{3/2}$ to selected $5p^46p$ states. The final states are grouped by their total electronic angular momentum, with $J = 7/2$ and $5/2$ shown in panel (a) and $J = 3/2$ and $1/2$ shown in (b).

section to be affected by whether or not the principal configuration of the core is changed. Generally, core-changing transitions are less likely than those that leave the core unchanged. In light of the complicated coupling scheme involved in the Xe^+ target states, however, it is by no means straightforward to derive a systematic rule that is valid for all circumstances.

Nevertheless, the above findings also apply to the $5p^46p$ states. In figure 4, the order of cross section peaks in the core group is $^3P > {}^1D > {}^1S$. Note, however, that the cross sections for energetically higher states can be larger than those of lower states within the same core group. Examples are $(^3P_1)6p\ [2]_{3/2}$ (energy 15.28 eV) and $(^3P_0)6p\ [1]_{1/2}$ (energy 14.93 eV) shown in figure 4(b). Hence, the energy position of a state is not the only deciding factor. Most likely, the number of magnetic substates, i.e., the degeneracy of the states, will have an effect as well.

The $5p^46p$ states of Xe^+ are important in optical emission spectroscopy (OES), because of their relatively strong emission lines in the wavelength range ~400–700 nm [20]. As will be shown in our next paper, 32 ionic lines of 6p–6s and 6p–5d transitions are observed in the emission spectra of Hall thrusters. Of these, 22 belong to states with a ^3P core and 10 to states with a ^1D core. No lines from 6p states with a ^1S core were found, hence implying very low densities of these states. This evidence agrees with the order of cross-section magnitudes discussed above.

3.3. Metastable and quasi-metastable state excitation

There are six metastable states in the Xe^+ ion that cannot decay by electric dipole transitions to lower states. All of them belong to the $5p^45d$ configuration. In contrast, the neutral Xe atom has only two metastable states in the $5p^56s$ configuration. In addition, there are several 'quasi-metastable' states in the $5p^46s$ and $5p^45d$ configurations of Xe^+. These states have relatively long lifetimes (e.g. ~1 μs) compared with the characteristic time of collisional transitions in Hall and ion thrusters (e.g. ~0.01–0.1 μs at plasma densities of $\sim 10^{12}\,cm^{-3}$). In this case, both the metastable and quasi-metastable states are mainly depopulated by electron-impact excitation processes to higher (e.g. 6p) states. Metastable- and quasi-metastable-state excitations become an important mechanism for their own kinetics as well as that of the 6p states involved in OES diagnostics.

Figures 5 and 6 depict the electron-impact excitation cross sections of ten $5p^46p$ states from the quasi-metastable state $5p^4(^3P_2)6s\ ^2[2]_{5/2}$ (the lowest state in the 6s/5d configurations) and the metastable state $5p^4(^3P_2)5d\ ^2[4]_{9/2}$ (the state with the highest degree of degeneracy in the 6s/5d configurations), respectively.

In the optical diagnostics of low-temperature plasmas, it is well understood that competition between ground-state excitation by high-energy electrons and metastable-state excitation by low-energy electrons is the essential physical reason why the OES line-ratio method can determine the mean electron energy or electron energy distribution function, when using a CR model for Ne, Ar, Kr, or Xe atoms [31–34]. Atomic states such as $np^5(^2P^o_{3/2})(n+1)p\ ^2[1/2]_0$ and $np^5(^2P^o_{3/2})(n+1)p\ ^2[5/2]_3$ are usually selected, since the former is mainly produced by excitation from the ground state $np^6\ (^1S_0)$ while the latter has large excitation cross sections from the dominant metastable state $np^5(^2P^o_{3/2})(n+1)s\ ^2[3/2]^o_2$. This is the well-known systematic behavior found in previous CR modelling and OES diagnostics research of low-temperature Ne, Ar, Kr and Xe plasmas.

However, when comparing the excitation cross sections of $Xe^+(6p)$ in figures 4–6, the situation is much more complex. For example, for the first three states, the order of cross sections is $(^3P_2)6p\ [3]_{7/2} > (^3P_2)6p\ [3]_{5/2} > (^3P_2)6p\ [2]_{5/2}$ for the ground-state excitation in figure 4(a), $(^3P_2)6p\ [3]_{7/2} > (^3P_2)6p\ [2]_{5/2} > (^3P_2)6p\ [3]_{5/2}$ for the metastable-

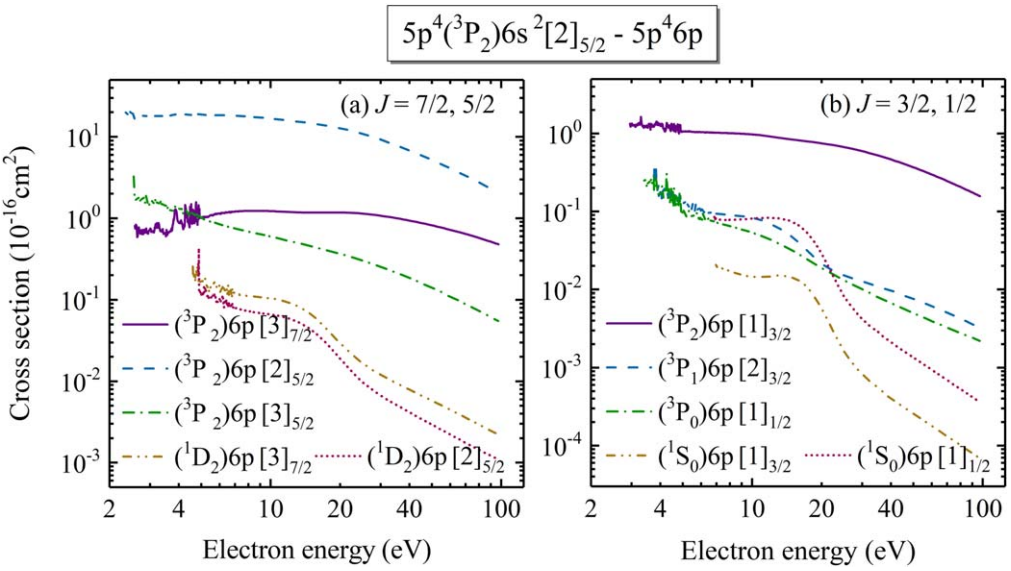

Figure 5. Electron-impact excitation cross sections for transitions from $5p^4(^3P_2)6s\ ^2[2]_{5/2}$ to selected $5p^4 6p$ states. As in figure 3, we group them according to the J-value of the final state, with $J = 7/2$ and $5/2$ shown in (a) and $J = 3/2$ and $1/2$ in (b).

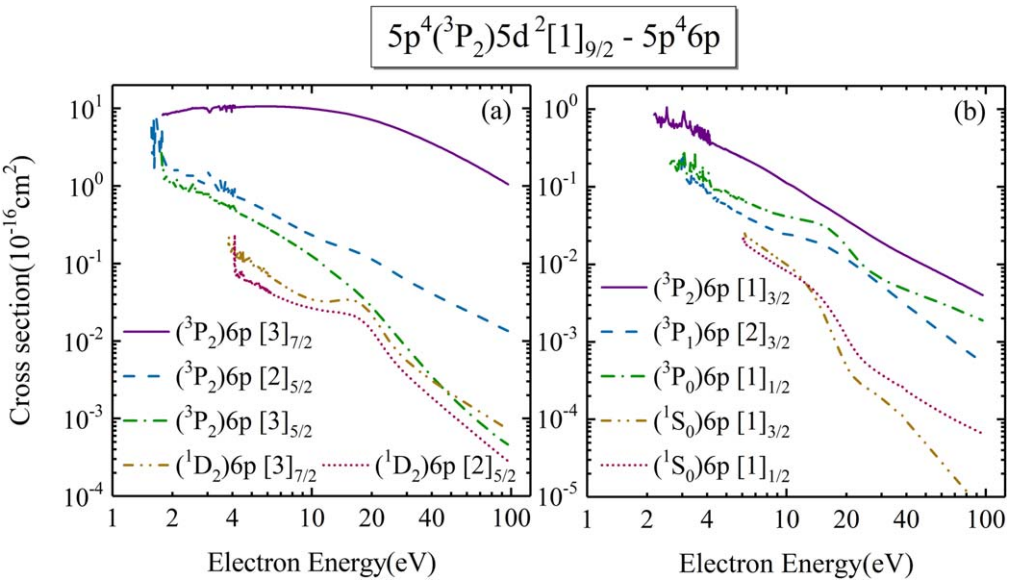

Figure 6. Electron-impact excitation cross sections for the transitions from $5p^4(^3P_2)5d\ ^2[4]_{9/2}$ to selected $5p^4 6p$ states with $J = 7/2$ and $5/2$ in panel (a) and $J = 3/2$ and $1/2$ in panel (b).

state excitation in figure 6(a) and $(^3P_2)6p\ [2]_{5/2} > (^3P_2)6p\ [3]_{5/2} > (^3P_2)6p\ [3]_{7/2}$ at low energy (~3 eV) and $(^3P_2)6p\ [2]_{5/2} > (^3P_2)6p\ [3]_{7/2} > (^3P_2)6p\ [3]_{5/2}$ at high energy (~30 eV) in figure 5(a) for the quasi-metastable-state excitation. The order is thus changed in each case.

Furthermore, there is a second fine-structure state ($5p^5\ ^2P^o_{1/2}$) with the ground-state configuration and about ten more metastable/quasi-metastable states should be considered for the production of $Xe^+(6p)$. The kinetic mechanisms become more complicated due to the high density and energy of electrons and ions in the electric propulsion systems, since electron-impact ionization–excitation (from the atomic ground state to excited ionic states), ion-impact excitation and ionization–excitation, and charge-transfer processes between the atom and the ion will compete with the above electron-impact excitation processes. The experience accumulated in the CR modeling of atoms during the past decade [32–37], therefore, may not be transferable in a straightforward way to a CR model of Xe^+. A comprehensive study of the kinetic processes involving the ionic 6s, 6p, and 5d states in the different regions of electric propulsion devices will be carried out by utilizing the cross-section data generated in the present work, and the results will be reported in a subsequent paper.

3.4. Limitations of the present calculation

In the present work, we focused on performing structure and collision calculations for the Xe^+ ion by using a 67-state DBSR model to generate a consistent set of Einstein coefficients and cross sections for our planned CR model. In

principle, more structure data could be provided, and we could further improve their accuracy in a more sophisticated structure-only calculation. Such refinements, however, lead to a major increase in the resource requirements for a subsequent collision calculation. They are beyond our current computational capabilities.

As a further limitation of the model, we note that neither the $5p^4 6d$ nor the $5p^4 4f$ states were included in the close-coupling expansion. The latter states are important for predicting the emission spectra of electric propulsion systems in the wavelength range ~200–300 nm[6]. Considering that the projectile electron would have to be coupled to these states, collision calculations involving the $5p^4 4f$ states would lead to a very large number of scattering channels and extensive interaction matrices, once again beyond currently available capabilities. Hence a compromise had to be made in the number of target configurations that could be considered.

4. Conclusions and outlook

In this work, the fully relativistic DBSR method was employed to calculate energy levels, oscillator strengths, and electron-impact excitation cross sections for the Xe^+ ion. These data are necessary for the kinetic modelling of excited Xe^+ ions in electric propulsion systems and for optical line-ratio diagnostics of Xe plasmas with the ionic emission lines included. The multi-electron Dirac-Coulomb Hamiltonian was used to comprehensively account for valence and core-valence correlations as well as relativistic effects for this heavy target. Utilizing nonorthogonal orbital sets, both for the construction of the target wave functions and the representation of the scattering functions, allowed us to optimize the individual wave functions independently, and hence to generate a more accurate description of the target than what is usually possible with orthogonal orbital sets, in particular if the target states are to be used in a subsequent collision calculation.

The oscillator strengths obtained in this work are in good agreement with those measured in different plasmas reported in the literature. The magnitude of the predicted cross sections also agrees with preliminary experimental observations of emission line intensities in Hall and ion thrusters. The accuracy of the data will be further examined by more detailed optical experiments in such thrusters. In spite of the major challenges outlined above, large-scale DBSR calculations with inclusion of the $5p^4 6d$ and $5p^4 4f$ states as well as accounting for coupling to the target continuum are envisioned for future work. The latter extension would also make it possible to treat ionization processes of excited Xe^+ states and to study the production mechanisms of Xe^{2+} and Xe^{3+} ions.

[6] For example, we observed a series of $Xe^+(4f)$ emission lines in this range when developing a novel type of magnetized hollow cathode thrusters. The ratio between these $Xe^+(4f)$ lines and the lines of boron, tantalum, and barium species is useful to monitor the performance of this kind of device and will be studied in future work.

Table A1. Energy levels of Xe^+ (in eV) relative to the ground state obtained in this work, compared with those in the NIST [20] tables (J denotes the total angular momentum quantum number).

No.	State	Term	J	This work	NIST
1	$5p^5$	$^2P^\circ$	3/2	0.000 00	0.000 00
2	$5p^5$	$^2P^\circ$	1/2	1.287 79	1.306 42
3	$5s5p^6$	^2S	1/2	11.3908	11.2669
4	$5p^4(^3P_2)6s$	$^2[2]$	5/2	12.1174	11.5390
5	$5p^4(^3P_2)6s$	$^2[2]$	3/2	12.4006	11.7865
6	$5p^4(^3P_2)5d$	$^2[2]$	5/2	12.5840	11.8277
7	$5p^4(^3P_2)5d$	$^2[3]$	7/2	12.5938	11.8328
8	$5p^4(^3P_2)5d$	$^2[2]$	3/2	12.6824	11.9066
9	$5p^4(^3P_2)5d$	$^2[1]$	1/2	12.7489	12.0088
10	$5p^4(^3P_0)6s$	$^2[0]$	1/2	13.0977	12.5419
11	$5p^4(^3P_2)5d$	$^2[4]$	9/2	13.1766	12.3247
12	$5p^4(^3P_1)6s$	$^2[1]$	3/2	13.3357	12.7455
13	$5p^4(^3P_2)5d$	$^2[4]$	7/2	13.4580	12.5888
14	$5p^4(^3P_1)6s$	$^2[1]$	1/2	13.5708	13.2547
15	$5p^4(^3P_2)5d$	$^2[1]$	3/2	13.8650	13.0572
16	$5p^4(^3P_1)5d$	$^2[1]$	1/2	13.8836	12.9254
17	$5p^4(^3P_2)5d$	$^2[0]$	1/2	14.0331	13.1358
18	$5p^4(^3P_2)5d$	$^2[3]$	5/2	14.0409	13.2012
19	$5p^4(^3P_0)5d$	$^2[2]$	3/2	14.1098	13.3136
20	$5p^4(^1D_2)6s$	$^2[2]$	5/2	14.1859	13.5841
21	$5p^4(^3P_2)6p$	$^2[2]^\circ$	3/2	14.2145	13.8605
22	$5p^4(^3P_1)5d$	$^2[1]$	3/2	14.2200	13.3785
23	$5p^4(^3P_2)6p$	$^2[2]^\circ$	5/2	14.2203	13.8811
24	$5p^4(^3P_1)5d$	$^2[3]$	7/2	14.2635	13.4428
25	$5p^4(^3P_0)5d$	$^2[2]$	5/2	14.3149	13.3912
26	$5p^4(^3P_2)6p$	$^2[3]^\circ$	5/2	14.4117	14.0737
27	$5p^4(^3P_2)6p$	$^2[1]^\circ$	1/2	14.4156	14.0936
28	$5p^4(^3P_2)6p$	$^2[3]^\circ$	7/2	14.4166	14.0977
29	$5p^4(^1D_2)6s$	$^2[2]$	3/2	14.5457	14.0009
30	$5p^4(^3P_1)5d$	$^2[2]$	3/2	14.7049	13.8028
31	$5p^4(^3P_2)6p$	$^2[1]^\circ$	3/2	14.8148	14.4793
32	$5p^4(^3P_1)5d$	$^2[2]$	5/2	14.8240	13.9735
33	$5p^4(^3P_1)5d$	$^2[3]$	5/2	14.9872	14.2273
34	$5p^4(^1D_2)5d$	$^2[4]$	9/2	15.0959	14.2464
35	$5p^4(^1D_2)5d$	$^2[4]$	7/2	15.1407	14.2475
36	$5p^4(^3P_0)6p$	$^2[1]^\circ$	1/2	15.2734	14.9295
37	$5p^4(^3P_1)6p$	$^2[0]^\circ$	1/2	15.3500	15.0244
38	$5p^4(^3P_0)6p$	$^2[1]^\circ$	3/2	15.4085	15.0801
39	$5p^4(^3P_1)6p$	$^2[2]^\circ$	5/2	15.5780	15.2640
40	$5p^4(^3P_1)6p$	$^2[2]^\circ$	3/2	15.6118	15.2816
41	$5p^4(^1D_2)5d$	$^2[3]$	5/2	15.6227	14.7647
42	$5p^4(^3P_1)6p$	$^2[1]^\circ$	3/2	15.7392	15.4099
43	$5p^4(^3P_1)6p$	$^2[1]^\circ$	1/2	15.7722	15.4448
44	$5p^4(^1D_2)5d$	$^2[3]$	7/2	15.8873	14.9839
45	$5p^4(^1D_2)5d$	$^2[2]$	5/2	16.1149	15.4115
46	$5p^4(^1D_2)5d$	$^2[1]$	3/2	16.1157	15.3827
47	$5p^4(^1D_2)5d$	$^2[1]$	1/2	16.3016	15.7473
48	$5p^4(^1D_2)6p$	$^2[3]^\circ$	5/2	16.3387	15.9775
49	$5p^4(^1D_2)6p$	$^2[1]^\circ$	3/2	16.4136	16.0767
50	$5p^4(^1D_2)6p$	$^2[3]^\circ$	7/2	16.4581	16.1259
51	$5p^4(^1D_2)5d$	$^2[2]$	3/2	15.5536	15.8114
52	$5p^4(^1S_0)6s$	$^2[0]$	1/2	16.6028	16.0248
53	$5p^4(^3P_2)7s$	$^2[2]$	5/2	16.6103	16.4302
54	$5p^4(^1D_2)6p$	$^2[2]^\circ$	3/2	16.7013	16.3565
55	$5p^4(^3P_2)7s$	$^2[2]$	3/2	16.7074	16.5134
56	$5p^4(^1D_2)6p$	$^2[2]^\circ$	5/2	16.7190	16.3917
57	$5p^4(^1D_2)6p$	$^2[1]^\circ$	1/2	16.7878	16.4578

Table A1. (Continued.)

No.	State	Term	J	This work	NIST
58	$5p^4(^3P_0)7s$	$^2[0]$	1/2	17.5304	17.4673
59	$5p^4(^1D_2)5d$	$^2[0]$	1/2	17.6631	16.7454
60	$5p^4(^3P_1)7s$	$^2[1]$	3/2	17.8187	17.6531
61	$5p^4(^1S_0)5d$	$^2[2]$	5/2	17.8997	16.9325
62	$5p^4(^3P_1)7s$	$^2[1]$	1/2	17.9027	17.7211
63	$5p^4(^1S_0)5d$	$^2[2]$	3/2	17.9925	17.1176
64	$5p^4(^1S_0)6p$	$^2[1]^\circ$	1/2	18.9002	18.3775
65	$5p^4(^1S_0)6p$	$^2[1]^\circ$	3/2	18.9147	18.4974
66	$5p^4(^1D_2)7s$	$^2[2]$	5/2	18.7487	18.5601
67	$5p^4(^1D_2)7s$	$^2[2]$	3/2	18.7850	18.5732

We are currently building a comprehensive collisional-radiative model for electric propulsion systems with Xe as the propellant—with the kinetics of metastable, quasi-metastable, and excited states of both the neutral atom and the ion included. Subsequent papers will focus on constructing this CR model and utilizing it for OES diagnostics, respectively.

All data generated in this project are available from the authors on request, and they are also put on the LXCat database, which is accessible at https://nl.lxcat.net/.

Acknowledgments

This work is supported by the National Natural Science Foundation of China under grant Nos. 11775063, 11404081, 51736003, and a research project under grant No. LabASP-2017-05. And by the United States National Science Foundation under grant Nos. PHY-1520970 (OZ and KB) as well as PHY-1403245 and PHY-1803844 (KB). The calculations were carried out on Stampede 2 at the Texas Advanced Computing Center at the University of Texas at Austin. They were made possible through the XSEDE supercomputer allocation TG-PHY-090031. One of us (KB) thanks his colleagues at the Harbin Institute of Technology for their hospitality during his visit.

Appendix A

Table A1 lists the energy levels studied in this work.

Appendix B

An excel file named 'CrossSectionsIon.xlsx' is attached as supplementary material is available online at stacks.iop.org/PSST/28/105004/mmedia, which is introduced in this appendix. It includes electron impact excitation cross sections of Xe^+ that are calculated by DBSR method. Only the data that are essential to build a collisional-radiative model in the follow-up paper are presented here, since a file contains all data generated in this work is too large to be an attached file. One can also find a full set of present DBSR calculations on the LXCat database, which is accessible at https://nl.lxcat.net/.

'CrossSectionsIon.xlsx' includes cross sections of transitions from two ground Xe^+ states ($J = 3/2$ and $J = 1/2$) to $5p^46s$, $5p^46p$, and $5p^45d$ states, as well as those from twelve metastable and quasi-metastable states (four $5p^46s$ states and eight $5p^45d$ states) to $5p^46p$ states. The theoretical data are stored in different worksheet according to the configurations of initial state and final state. For example, the data for transitions from ground state to $5p^46s$ are stored in worksheet 'gs -> 6s'.

In the excel file, for simplicity, transitions are described using NIST energy-ordered level numbers instead of level symbols. For example, in 'CrossSectionsIon.xlsx', transition '1 -> 4' in worksheet 'gs -> 6s' denotes transition from level No. 1 to level No. 4, where level No. 1 is actually the lowest Xe^+ level $5p^5\ ^2P_{3/2}$, and level No. 4 is $5p^4(^3P_2)6s\ ^2[2]_{5/2}$. In the subsequent paper of this series of work, energy levels are also quoted by NIST energy-ordered numbers. An energy-ordered level table can be found in worksheet 'NIST Level table' of each file. Energies of incident electron are given in eV, and cross sections are given in $10^{-16}\,cm^2$ in the file.

ORCID iDs

Yan-Fei Wang https://orcid.org/0000-0002-9226-8279
Xi-Ming Zhu https://orcid.org/0000-0002-6501-0096
Klaus Bartschat https://orcid.org/0000-0001-6215-5014

References

[1] Goebel D M and Katz I 2008 *Fundamentals of Electric Propulsion: Ion and Hall Thrusters* (New York: Wiley)
[2] Boeuf J-P 2017 Tutorial: physics and modeling of Hall thrusters *J. Appl. Phys.* **121** 011101
[3] Sutton G P and Biblarz O 2010 Rocket Propulsion Elements (New York: Wiley)
[4] Zhu X M and Pu Y K 2010 Optical emission spectroscopy in low-temperature plasmas containing argon and nitrogen: determination of the electron temperature and density by the line-ratio method *J. Phys. D: Appl. Phys.* **43** 403001
[5] Donnelly V M 2004 Plasma electron temperatures and electron energy distributions measured by trace rare gases optical emission spectroscopy *J. Phys. D: Appl. Phys.* **37** R217
[6] Boffard J B, Lin C C and Wendt A E 2018 Application of excitation cross-section measurements to optical plasma diagnostics *Adv. Atom. Mol. Opt. Phys.* **67** 1–76
[7] Zhu X M, Chen W C, Li J and Pu Y K 2009 Determining the electron temperature and the electron density by a simple collisional-radiative model of argon and xenon in low-pressure discharges *J. Phys. D: Appl. Phys.* **42** 025203
[8] Hill K W *et al* 1999 Tests of local transport theory and reduced wall impurity influx with highly radiative plasmas in the Tokamak fusion test reactor *Phys. Plasmas* **6** 877
[9] Yüce K, Castelli F and Hubrig S 2011 Wavelengths and oscillator strengths of Xe II from the UVES spectra of four HgMn stars *Astron. Astrophys.* **528** A37

[10] Di Rocco H O, Cruzado A and Marchiano P E 2015 On the line shift and oscillator strength of Xe II lines in the spectra of HnMn stars *Astron. Astrophys.* **581** A63
[11] Jung R O *et al* 2005 Electron-impact excitation cross sections from the xenon J = 2 metastable level *Phys. Rev.* A **72** 022723
[12] Chiu Y H *et al* 2006 Passive optical diagnostic of Xe-propelled Hall thrusters. I. Emission cross sections *J. Appl. Phys.* **99** 113304
[13] Srivastava R, Stauffer A D and Sharma L 2006 Excitation of the metastable states of the noble gases *Phys. Rev.* A **74** 012715
[14] Jung R O *et al* 2009 Excitation into $5p^5 7p$ levels from the ground level and the J = 2 metastable level of Xe *Phys. Rev.* A **80** 062708
[15] Zatsarinny O and Bartschat K 2010 Benchmark calculations for near-threshold electron- impact excitation of krypton and xenon atoms *J. Phys. B: At. Mol. Opt. Phys.* **43** 074031
[16] Priti, Gangwar R K and Srivastava R 2019 Collisional-radiative model of xenon plasma with calculated electron-impact fine structure excitation cross-sections *Plasma Sources Sci. Technol.* **28** 025003
[17] Gigosos M A *et al* 1994 Experimental Stark widths and shifts and transition probabilities of several Xe II lines *Phys. Rev.* E **49** 1575
[18] Zielińska S, Bratasz Ł and Dzierżęga K 2002 Absolute transition rates for transitions from $5p^4(^3P)6p\ ^4P^\circ_{5/2}$, $^4P^\circ_{3/2}$, $^4D^\circ_{7/2}$ and $^2D^\circ_{5/2}$ levels of Xe II *Phys. Scr.* **66** 454
[19] Di Rocco H O, Iriarte D I and Pomarico J A 2000 Lifetimes and transition probabilities of Xe II: experimental measurements and theoretical calculations *Eur. Phys. J.* D **10** 19
[20] NIST atomic spectra database 2018 https://nist.gov/pml/atomic-spectra-database
[21] Bertuccelli G and Di Rocco H O 1996 The measurements of transition probabilities using pulsed capillary discharges *J. Quant. Spectrosc. Radiat. Transf.* **55** 463
[22] Martín I *et al* 1999 Transition probabilities for singly ionized xenon *J. Quant. Spectrosc. Radiat. Transf.* **62** 71
[23] Gupta S, Sharma L and Srivastava R 2018 Electron-impact excitation of Xe + and polarization of its subsequent emissions *J. Quant. Spectrosc. Radiat. Transf.* **219** 7–22
[24] Zatsarinny O and Bartschat K 2009 B-spline calculations of oscillator strengths in noble gases *Phys. Scr.* **T134** 014020
[25] Zatsarinny O 2006 BSR: B-spline atomic R-matrix codes *Comput. Phys. Commun.* **174** 273
[26] Zatsarinny O and Bartschat K 2008 Relativistic B-spline R-matrix method for electron collisions with atoms and ions: application to low-energy electron scattering from Cs *Phys. Rev.* A **77** 062701
[27] Zatsarinny O and Bartschat K 2013 The B-spline R-matrix method for atomic processes: application to atomic structure, electron collisions, and photoionization *J. Phys. B: At. Mol. Opt. Phys.* **46** 112001
[28] Ning Z, Liu H, Yu D and Zhou Z 2011 Effects of ionization distribution on plasma beam focusing characteristics in Hall thrusters *Appl. Phys. Lett.* **99** 221502
[29] Kim H, Lim Y, Choe W and Seon J 2014 Effect of multiply charged ions on the performance and beam characteristics in annular and cylindrical type Hall thruster plasmas *Appl. Phys. Lett.* **105** 144104
[30] Lim Y *et al* 2017 Nonlinear ion dynamics in Hall thruster plasma source by ion transit-time instability *Plasma Sources Sci. Technol.* **26** 03LT01
[31] Zhu X M *et al* 2012 Possibilities of determining non-Maxwellian EEDFs from the OES line-ratios in low-pressure capacitive and inductive plasmas containing argon and krypton *Plasma Sources Sci. Technol.* **21** 024003
[32] Dressler R A *et al* 2009 Near-infrared collisional radiative model for Xe plasma electrostatic thrusters: the role of metastable atoms *J. Phys. D: Appl. Phys.* **42** 185203
[33] Boffard J B, Wang S, Lin C C and Wendt A E 2015 Detection of fast electrons in pulsed argon inductively coupled plasmas using the 420.1–419.8 nm emission line pair *Plasma Sources Sci. Technol.* **24** 065005
[34] Boffard J B, Jung R O, Lin C C and Wendt A E 2010 Optical emission measurements of electron energy distributions in low-temperature argon inductively coupled plasmas *Plasma Sources Sci. Technol.* **19** 065001
[35] Zhu X M and Pu Y K 2008 Using OES to determine electron temperature and density in low-pressure nitrogen and argon plasmas *Plasma Sources Sci. Technol.* **17** 024002
[36] Kano K, Suzuki M and Akatsuka H 2000 Spectroscopic measurement of electron temperature and density in argon plasmas based on collisional-radiative model *Plasma Sources Sci. Technol.* **9** 314
[37] Rolin M N, Shabunya S I, Rostaing J C and Prerrin J M 2007 Self-consistent modelling of a microwave discharge in neon and argon at atmospheric pressure *Plasma Sources Sci. Technol.* **16** 480